Journal of Power Sources 196 (2011) 10704–10711

Contents lists available at SciVerse ScienceDirect

Journal of Power Sources

journal homepage: www.elsevier.com/locate/jpowsour

Direct synthesis of nanostructured V_2O_5 films using solution plasma spray approach for lithium battery applications

Vikram Varadaraajan[a], B.C. Satishkumar[a,*], Jagjit Nanda[b], Pravansu Mohanty[a,**]

[a] Department of Mechanical Engineering, University of Michigan-Dearborn, Dearborn, MI 48128, USA
[b] Materials Science and Technology Division, Oak Ridge National Laboratory, Oak Ridge, TN 37831, USA

ARTICLE INFO

Article history:
Received 22 July 2011
Received in revised form 27 August 2011
Accepted 9 September 2011
Available online 16 September 2011

Keywords:
Li batteries
Energy storage
V_2O_5
Nanoparticles
Nanorods
Plasma spray deposition

ABSTRACT

We demonstrate for the first time, the synthesis of vanadium pentoxide (V_2O_5) nanoparticles and nanorods in the films using a high throughput solution plasma spray deposition approach. The scalable plasma spray method enables the direct deposition of large area nanostructured films of V_2O_5 with controllable particle size and morphology. In this approach, the solution precursors (vanadium oxychloride and ammonium metavanadate) were injected externally into the plasma jet, which atomizes and pyrolyzes the precursors in-flight, resulting in the desired films on the current collectors. The microstructure analysis of the as synthesized films revealed pure nanocrystalline phase for V_2O_5 with particles in the size range of 20–50 nm. The V_2O_5 film based electrodes showed stable reversible discharge capacity in the range of 200–250 mAh g^{-1} when cycled in the voltage window 2–4 V. We further discuss the mechanism for controlling the particle growth and morphology, and also the optimization of reversible lithium storage capacity. The nanorods of V_2O_5 formed after the anneal treatment also show reversible storage capacity indicative of the potential use of such film based electrodes for energy storage.

1. Introduction

Increasing need for electrical energy storage devices in daily life calls for rechargeable Li battery electrode materials which possess high energy density and high discharge capacity [1]. The most widely used commercial cathode based on $LiCoO_2$ exhibits a practical capacity at ~140 mAh g^{-1} [2], and is currently being substituted by other chemistries because of higher cost of cobalt and safety reasons, for example, $LiFePO_4$ [3–5]. There is a need for the materials which have high specific discharge capacity. In this regard cathode materials based on V_2O_5 and lithium vanadium oxides offer a promising alternative [6–8]. Although V_2O_5 offers high theoretical capacity, around ~440 mAh g^{-1}, the material limitations such as structural modification associated with lithium insertion, poor electronic conductivity [9] and low diffusion rate [10] prevent us from the full capacity realization. One of the approaches to overcome these limitations is focused towards the microstructural control of the particle phase and morphology, while at the same time maintaining the particle size in the nanometer regime to improve the lithium diffusion rate. Lithium insertion–deinsertion into V_2O_5 phases involves several complex structural phase modifications that are clearly manifested as plateaus during the charge discharge cycling. Typically the electrochemical reaction during Li insertion into V_2O_5 proceeds as,

$$V_2O_5 + xe^- + xLi^+ \rightarrow Li_xV_2O_5; \quad 0 < x \leq 3 \tag{1}$$

Depending on the amount of lithium intercalated inside the V_2O_5 structure it forms different structural phases, namely α, ε, δ, γ and *w*-$Li_xV_2O_5$ within the compositional range $0 < x \leq 3$ [11–13].

In this study we report for the first time the successful plasma spray deposition of nanostructured films of V_2O_5 using solution precursors. The plasma spray method has been developed over the years in our laboratory and has been successfully used for the deposition of adherent coatings and films of a variety of materials [14–17] using the liquid precursors. In order to get the correct phase and stoichiometry the choice of the solution precursor is crucial. To this effect we selected vanadium oxychloride and ammonium metavanadate; where the Vanadium is already in +5 oxidation state. Using this approach we achieve the appropriate material chemistry in flight and simultaneously consolidate the electrode films directly onto the current collector. The advantages with our current approach are one step synthesis and consolidation, large area deposition capability, without the further need for powder handling. Furthermore, the deposited films exhibit desired nanoparticulate matrix and through the control of plasma power, precursor feed rate and related plasma parameters we could rapidly

* Corresponding author. Present address: Advanced Engineering Center, Ford Motor Co., 2400 Village Rd., Dearborn, MI 48121, USA.
** Corresponding author.
E-mail addresses: satishbc@gmail.com (B.C. Satishkumar), pmohanty@umich.edu (P. Mohanty).

0378-7753/$ – see front matter © 2011 Elsevier B.V. All rights reserved.
doi:10.1016/j.jpowsour.2011.09.016

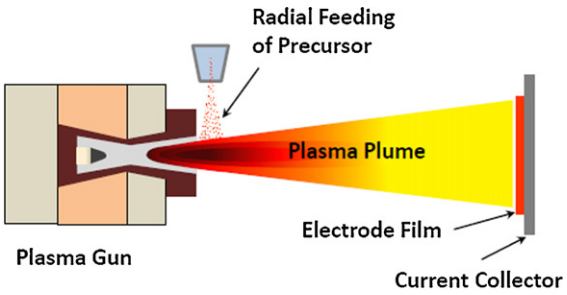

Fig. 1. Schematic of the setup for solution plasma spray deposition using 100HE Plasma Gun. The solution precursor is injected externally into the plasma flame and the desired material is deposited as a film on the substrate.

Fig. 2. The photographic image of as-sprayed V_2O_5 film (without binder and carbon) obtained by plasma spray deposition using solution precursor, $VOCl_3$.

deposit large area films of thickness ranging between 10 and 50 μm. For electrochemical testing the plasma spray deposited V_2O_5 films on Al discs were casted into electrodes by treatment with a solution of binder and conducting carbon black. The electrochemical properties of V_2O_5 films showed reversible capacity of ~230 mAh g^{-1}. Also, the plasma spray deposited V_2O_5 films were annealed at 400–600 °C in air to further investigate the microstructure transformation and evaluate their electrochemical properties. We notice that annealing helps in optimizing the microstructure and results in the formation of V_2O_5 nanorods and they exhibit significant improvement in the electrochemical properties for electrodes.

2. Experimental

2.1. Synthesis and characterization of V_2O_5 films

The DC plasma torch employed was based on 100 HE Plasma Gun (Progressive Technologies, Grand Rapids, MI, USA) modified to enable injection and atomization of solution precursors. The schematic of the plasma spray set up used in present studies is shown in Fig. 1. The solution precursor was injected normal to the plasma plume (also referred to as external or radial injection) similar to the conventional powder fed plasma spray processes (see Fig. 1). The working range of the gun is 210–250 V, with plasma current up to 350 A. The plasma gases used are a mixture of argon/nitrogen/hydrogen. The films were deposited on the as received 0.406 mm aluminum or stainless steel sheets (from McMaster Carr, USA). The parameters used for V_2O_5 film deposition are listed in Table 1. The standoff distance was varied between 125 and 175 mm and a constant 25 mm s^{-1} traverse speed was used for all the depositions.

First, as received vanadium trichloride oxide ($VOCl_3$, 28% from Alfa Aesar) was atomized using a custom designed nozzle-reservoir arrangement. Subsequently, ammonium vanadium oxide (NH_4VO_3, 99% from Alfa Aesar) was dissolved using oxalic acid (10% from Alfa Aesar) and the solution was used for spraying. Also, for comparison we sprayed the commercial V_2O_5 powder (99% from Alfa Aesar) to obtain the film coatings. Throughout the spray process, the feed rate for the solution (~10 ml min^{-1}) was kept constant. The precursor decomposition was optimized to yield V_2O_5 films and in the present studies we carried out the deposition using the plasma power in the range 60–70 kW.

As-sprayed V_2O_5 films were annealed in air in the temperature range 400–600 °C for 2–4 h or 700 °C for 15–30 min. The annealing treatment leads to weight loss (~10–20%), which could be attributed to conversion of any residual unconverted precursor that may be present in the as-sprayed films. The plasma spray deposited and annealed V_2O_5 films were characterized using X-ray diffraction (radiation Cu Kα = 1.54 Å) using Rigaku Miniflex diffractometer. The microstructure of the films was investigated using Hitachi H2600N scanning electron microscope (SEM) and Hitachi HT-7700 transmission electron microscope (TEM). Thermogravimetric analysis (TGA) of the V_2O_5 films was carried out using TA Instruments Q600.

2.2. Electrochemical testing of V_2O_5 films

For the electrochemical testing, both as-sprayed and annealed V_2O_5 films were casted into electrodes by soaking in a solution mixture of binder and carbon black. Specifically, we made use of polyvinylidenefluoride (PVDF, Kynar HSV 900 from Arkema Inc) and polyacrylic acid (PAA, from Sigma Aldrich Co) as binders which were dissolved respectively in 1-methyl-2-pyrrolidinone (99.5%, from Sigma Aldrich Co) and isopropanol (anhydrous, from Alfa Aesar). The binder mixing ratio was about 3–5% w/v PVDF or PAA, and carbon black (obtained from Super P, from Timcal USA Inc, 5–10% w/v) was added to the binder solution. Both as-sprayed and annealed V_2O_5 films (on Al substrates) were soaked in the solution mixture of binder and carbon black for 5–6 h. Later V_2O_5 films coated with binder and carbon black were annealed in vacuum oven at 110 °C for 12–15 h. The film based electrodes were later tested with thin foil of Li (from FMC Lithium) as counter and reference electrode in a flat cell (from MTI Inc, USA). Celgard 2400 (from Celgard Inc) membranes made of polypropylene were used as the separator and 1 M $LiPF_6$ (from Novolyte Inc) dissolved in 1:1 ethylene carbonate/dimethyl carbonate (from Novolyte Inc) was used as an electrolyte. AC impedance spectra of V_2O_5 films without and with binder/carbon were measured in order to establish electrode film characteristics (see Supplementary information). The electrochemical studies such as cyclic voltammetry (CV) and charge–discharge cycling were carried out using BioLogic multichannel work-station. For cyclic voltammetry studies the cells were cycled in the potential range 2–4 V at scan rate of 0.1 mV s^{-1}. Galvanostatic charge–discharge cycling studies were carried out in the potential range 2–4 V. We made use of Al discs (1 cm × 1 cm) with V_2O_5 films for the charge–discharge testing. The active material weights were measured by careful scraping of V_2O_5 and weighing inside the balance attached to TGA Q600. The microbalance is suitable for measuring weights with high accuracy. The active material loading in the 1 cm^2 Al discs is in the range 1.5–2.0 mg (does not include the weight of carbon black and binder).

3. Results and discussion

3.1. Structure and microstructure characterization

The photographic image of the large area V_2O_5 film deposited on Al (see Fig. 2) illustrates the capability of large area patterning of the electrodes on the current collector (Al). The image shows the bright yellow colored V_2O_5 film deposited on the aluminum substrate. The plasma spray deposited films of V_2O_5 show the desired orthorhombic phase, as illustrated in the XRD patterns shown in Fig. 3. We show the XRD patterns for V_2O_5 films obtained using

Table 1
List of plasma spray process parameters used for the deposition of V_2O_5 films.

Plasma spray condition	Standoff (mm)	Current (A)	$Ar/N_2/H_2$ (SLPM[a])	Power (kW)	Liquid feed rate (ml min^{-1})	Raster speed (mm s^{-1})	Cycles
1	125	250	85/40/55	65	15	25	15
2	175	250	85/40/55	65	15	25	15
3	175	225	85/40/55	60	15	25	10
4	175	275	85/40/55	70	15	25	10

[a] SLPM: standard litter per minute.

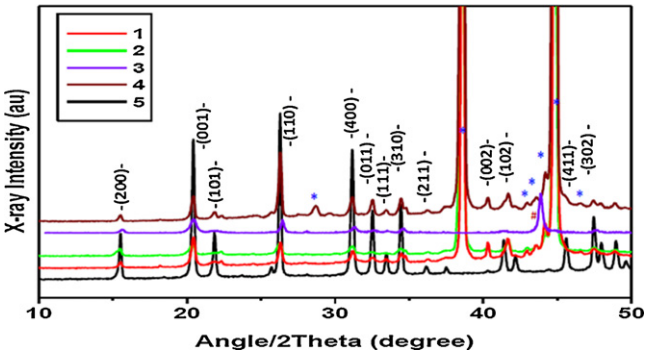

Fig. 3. XRD patterns of the films of V_2O_5 deposited through solution plasma spray approach on Al and stainless steel substrates. The V_2O_5 films obtained using precursor $VOCl_3$ (graphs-1 and 2, obtained at 60 kW and 65 kW respectively), NH_4VO_3 (graph-3, obtained at 60 kW), after anneal treatment at 600 °C for 1 h (graph-4) and commercial powder precursor (graph-5) are shown. The peaks marked by * and # refer to Al and stainless steel substrate reflections respectively.

two different precursors, vanadium oxychloride (see red and green curves, obtained at 60 kW and 65 kW respectively) and ammonium metavanadate (see purple graph in Fig. 3, obtained at 60 kW). The choice of these precursors was based on the fact that the vanadium ions are in +5 oxidation state, same as the end product V_2O_5 and hence excludes any formation of phases with lower oxidation state, such as V_2O_3. Among the two solution precursors the oxychloride worked better as it could be sprayed directly, while the metavanadate needed dissolution in oxalic acid and concentration limits the thickness for the V_2O_5 films. The plasma spray deposited V_2O_5 films were annealed in air for further studies. We show the XRD pattern for V_2O_5 film annealed at 600 °C for 1 h (see brown graph in Fig. 3). The XRD pattern of the commercial V_2O_5 powder (see black curve) is also shown for reference. The as-sprayed and annealed films show the desired orthorhombic phase for V_2O_5 (ICDD PDF # 00-41-1426). The microstructure of the films is illustrated in the SEM micrographs shown in Fig. 4(a) and (b). The images show the porous structure for the V_2O_5 films (see Fig. 4(a)) and the films consist of very fine nanoparticles, which form the aggregates (see Fig. 4(b)). This is generally the case for microstructure of films obtained using the solution precursors. In order to illustrate the unique advantage of our solution plasma spray approach we carried out deposition using the commercial V_2O_5 powder as a precursor. The V_2O_5 commercial powder comprises of particles with larger size (diameter: 20–50 μm and length: 100–150 μm). During the deposition the powder was directly fed externally into the plasma and such film coatings show entirely different microstructure. The plasma spray deposition using commercial V_2O_5 powder resulted in dark purple colored films. The SEM images of the films (see Fig. 4(c) and (d)) show elongated rod shaped structures which are

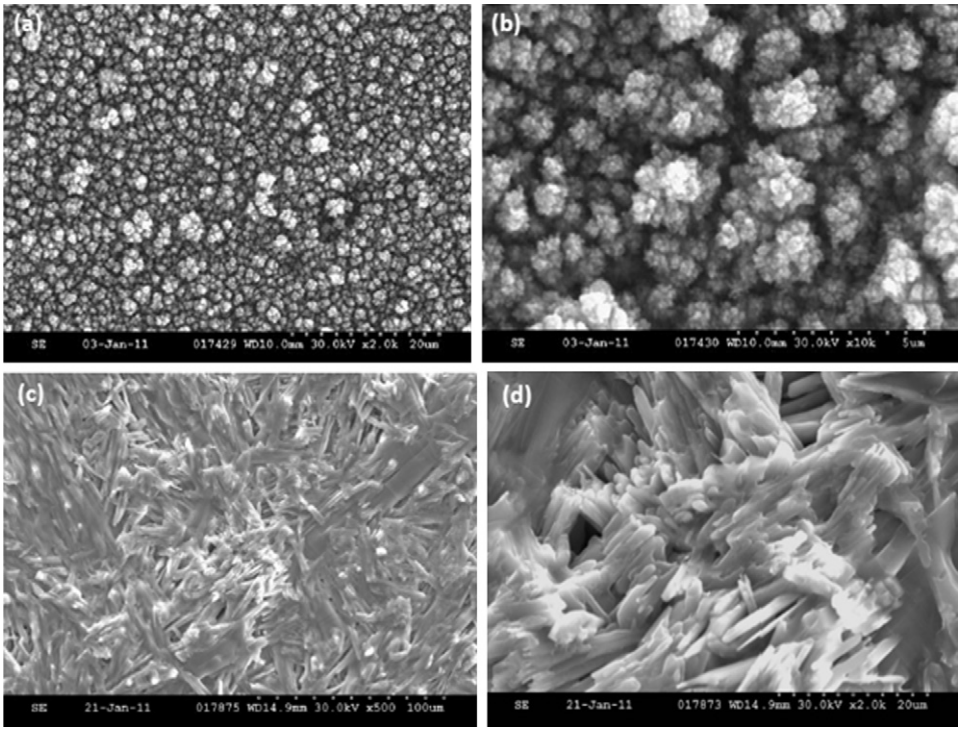

Fig. 4. (a) and (b) show SEM micrographs of plasma spray deposited V_2O_5 films using solution precursor, $VOCl_3$. The porous microstructure shows aggregates of V_2O_5 nanoparticles, (c) and (d) show the SEM micrographs of the V_2O_5 films obtained by the plasma spray deposition of the commercial V_2O_5 powder. The micron size rod shaped structures of V_2O_5 were observed.

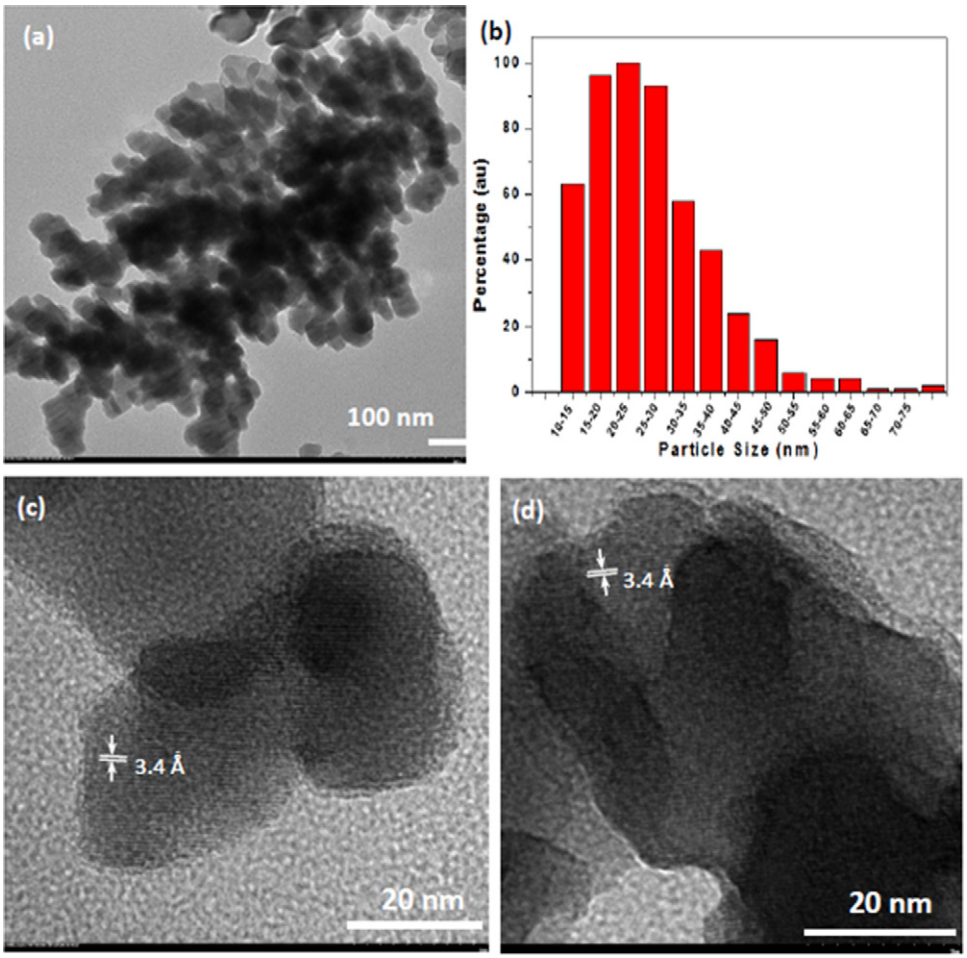

Fig. 5. (a) TEM image of V_2O_5 nanoparticles formed in the plasma spray deposited films, (b) shows the nanoparticle size distribution in as-sprayed V_2O_5 films, obtained using $VOCl_3$ precursor, (c) and (d) show the high resolution TEM images of the as-sprayed V_2O_5 films illustrating the nanoparticles of oxide with lattice resolution. The lattice planes exhibit a lattice spacing of ~3.4 Å which correspond to (1 1 0) planes.

stacked together. The diameter of rod shaped structures is typically in the range 0.5–3.0 μm and they are they are 15–20 μm long. The XRD studies of films derived from powder spray approach showed a mixture of phases (data not shown). These studies demonstrate the advantage of using the solution based precursors for the plasma deposition employed in the present studies. The solution precursors offer far greater control over the size of particles formed during the plasma spray deposition. In this deposition scheme, the atomized solution precursor undergoes pyrolysis during its flight inside the plasma plume. As a result, the precursor transforms into clusters of nanoscale oxide particles which are deposited as a film on the substrate. The proposed reaction mechanism for conversion of solution precursors could proceed as given in the reaction scheme shown below,

$$2VOCl_3 + 2O_2 \rightarrow V_2O_5 + 3Cl_2 + \frac{1}{2}O_2 \quad (2)$$

$$2NH_4VO_3 \rightarrow V_2O_5 + 2NH_3 + H_2O \quad (3)$$

The TEM observations of the as-sprayed films show the nanoparticulate structure of the films in further detail. The nanoparticles of the oxide are crystalline and exhibit uniform size (see Fig. 5(a)). The selected area diffraction studies on the V_2O_5 nanoparticles show the spotted ring patterns (not shown). We carried out the histogram analysis of the nanoparticles from the films during the TEM observations, and the size distribution is shown in Fig. 5(b). The nanoparticle size distribution is in the broad range of 20–50 nm, which is highly desired for the energy storage applications. The greatest advantage of solution plasma approach is that the solution precursor gives rise to very fine nanoparticles upon decomposition inside the plasma. This approach is far superior to the powder spray approach, as the starting powders dictate the size of particles in the deposited films. It should also be noted that plasma spraying of very fine pre-synthesized powders is extremely difficult due to mechanical challenges associated with feeding. Further, these nanoparticles tend to coalesce in-flight and lose their particulate size advantages. The high resolution TEM images of the nanoparticles show the crystalline lattice structure (see Fig. 5(c) and (d)). The nanoparticles are single crystalline and show lattice planes of V_2O_5 with interplanar spacing of 3.42 Å, which correspond to (1 1 0) crystallographic planes. Some of the nanoparticles show amorphous regions. These regions may be due to partially converted precursors as referred to the mass loss observed in the anneal studies. The observation of amorphous nanoparticles could be attributed to the fact that during thermal spray process the material undergoes rapid cooling. The XRD studies, however, show crystalline reflections for the films and therefore the amorphous content appears to be minimal.

We annealed the as-sprayed V_2O_5 films in order to investigate the structure transformation of the nanoparticles. After the anneal treatment the film microstructure shows modification, wherein, the nanoparticles of oxide transform into nanorod shaped structures. The SEM images of annealed films show the abundance of V_2O_5 nanorods (see Fig. 6(a) and (b)). The V_2O_5 nanorods exhibit growth in size with anneal time during the heat treatment at 700 °C.

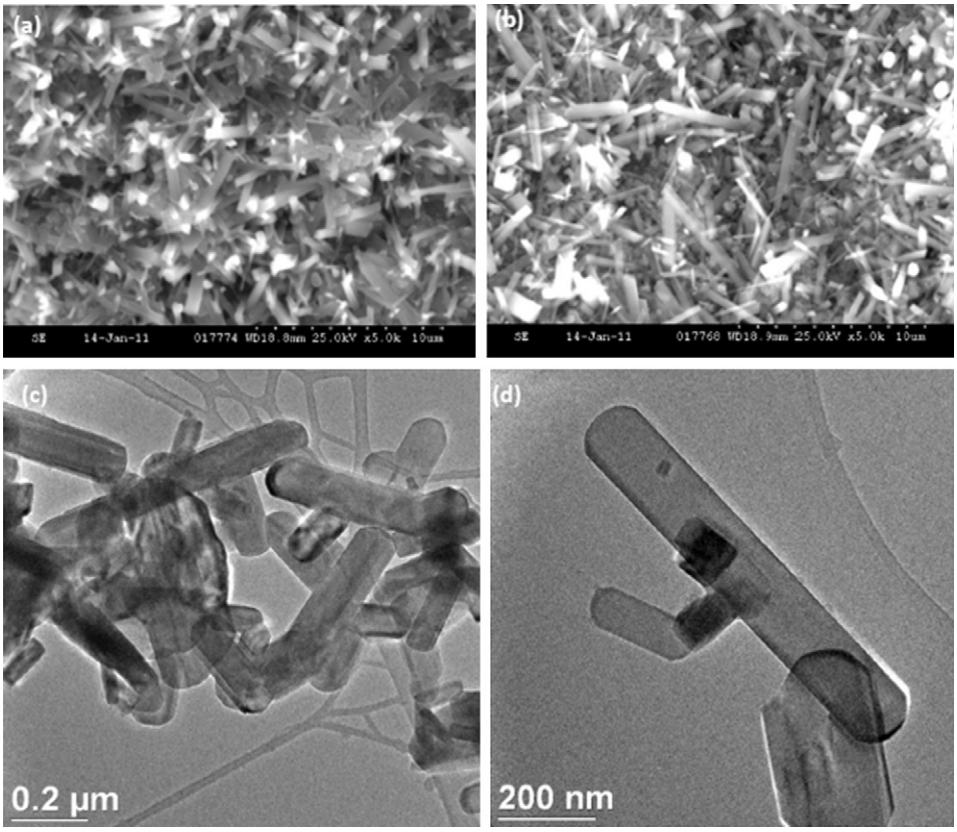

Fig. 6. SEM micrographs of V_2O_5 films annealed in air at 700 °C for (a) 15 min and (b) 30 min. The annealed films show the abundance of V_2O_5 nanorods, (c) and (d) show TEM images of V_2O_5 nanorods formed after the heat treatment of as-sprayed films at 500 °C for 4 h in air.

They are typically short (~5–6 μm) when annealed at 700 °C for 15 min (as shown in Fig. 6(a)), and grow longer (up to 10 μm) after the anneal treatment at 700 °C for 30 min (see Fig. 6(b)). The diameter of the nanorods shown in Fig. 6(a) and (b) is in the range 150–300 nm and they are up to 10 microns in length. The microstructure of annealed V_2O_5 films was investigated in a TEM. The V_2O_5 nanorods formed after the anneal treatment of as-sprayed films at 500 °C for 4 h are shown in the TEM images in Fig. 6(c) and (d). The diameter of V_2O_5 nanorods formed during such an anneal treatment is in the range 100–200 nm. The detailed mechanism of nanoparticles transforming into nanorods during the anneal treatment needs further studies. Nevertheless, the observation of V_2O_5 nanorod formation is advantageous because the effect of size and structure on the electrochemical properties could be further evaluated.

3.2. Cyclic voltammetry studies

The cyclic voltammetry studies carried out on the V_2O_5 film based electrodes show the redox reaction characteristics during the Li insertion/extraction process. The CV graphs obtained at scan rate, 0.1 mV s^{-1} are shown for as-sprayed and annealed (600 °C for 1 h) V_2O_5 films in Fig. 7(a) and (b) respectively. Both as-sprayed and annealed V_2O_5 films exhibit the oxidation/reduction features (shown by black and red arrows) which characterize the extraction/insertion of Li ions respectively. The peak positions during oxidation (Li extraction) are located at 2.59 V, 3.40 V and 3.54 V. During the lithium insertion process into V_2O_5 nanorods the CV scans show peaks at 3.33 V, 3.05 V and 2.19 V (see Fig. 7(b)). These peaks result from the various lithiated phases formed during the cathodic scan. V_2O_5 undergoes lithiation to form the lithiated phases, ε-$Li_{0.5}V_2O_5$, δ-LiV_2O_5 and γ-$Li_2V_2O_5$ [11,13,18–20], and the observed peaks correspond to the respective phases. The V_2O_5 nanorods in the annealed films show sharper and well resolved features relative to the nanoparticles. We propose that the nanorods formed after the anneal process show better kinetics during the Li insertion and extraction process. More studies on lithium diffusion rates could elucidate the kinetics in the plasma spray deposited nanostructured V_2O_5 films. The peak positions for the oxidation/reduction features indicate the very fine nanosize features for both the nanoparticles and the nanorods in our V_2O_5 films. The particle size in V_2O_5 electrodes affects the redox reaction during the Li extraction/insertion process [11,20,21], and fine nanoparticles and nanorods are desired to achieve faster kinetics during the cycling process. Electrodes based on nanostructured materials have been shown to facilitate faster Li transport, because of high surface area, and this in turn helps to achieve higher rate capabilities [20–24]. For V_2O_5 electrodes, lithium transport is facilitated in the a–b plane which can accommodate the Li ions inside the layers [11,25]. The layered structure of V_2O_5 is due to weak V–O bonds along the c-axis and the lithiated phases undergo structure transformation [11].

3.3. Charge–discharge and cycling studies

The galvanostatic charge–discharge studies were carried out on the V_2O_5 film electrodes using low current density. The charge–discharge data for as-sprayed and annealed (600 °C for 1 h) V_2O_5 films (with binder and carbon black, see experimental details) are shown in Fig. 8(a) and (b) respectively. Pristine or as-deposited V_2O_5 films exhibit poor electronic conductivity and carbon addition is necessary to enhance conductivity for the electrochemical studies [9,26] (see Supplementary information for AC impedance studies on films without and with binder/carbon), and, the binder matrix provides mechanical or physical support

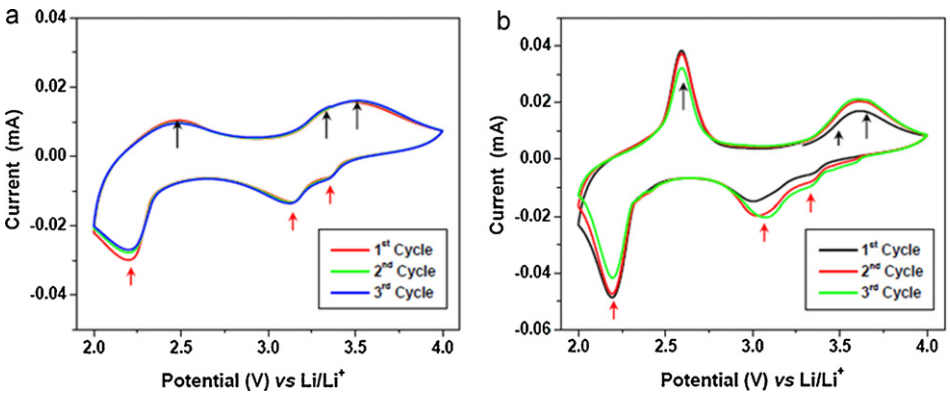

Fig. 7. CV graphs showing the first three cycles of electrodes from (a) as-sprayed V_2O_5 film and (b) V_2O_5 film annealed at 600 °C for 1 h, obtained at scanning rate of 0.1 mV s^{-1}.

to the active material (i.e. V_2O_5) during repeated electrochemical cycling. The data shows the charge–discharge behavior for 1st cycle (black graphs) and 20th cycle (red graphs). Both the as-sprayed and annealed V_2O_5 films show the characteristic two plateaus in the voltage ranges 2.2–2.4 V and 3.2–3.3 V during the discharge cycle. These features arise during the structure transformation of lithiated phases, ε-$Li_{0.5}V_2O_5$, δ-LiV_2O_5 and γ-$Li_2V_2O_5$ in the order ε/δ and δ/γ for two-phase regions [11]. The capacity decreases by ~8% at the end of 20 cycles for the as-sprayed V_2O_5 films, while the annealed films show a capacity drop of ~10%. In our studies, we observed that polyacrylic acid (PAA) works better relative to PVDF used as a filler for the films. The role of PAA is that it acts as a polyelectrolyte and assists in Li ion transport, while PVDF is just a binder holding the active electrode material and the carbon black. The cycling studies were carried out using current density of around ~0.025 mA cm^{-2}. The cycling characteristics of the as-sprayed (see black graph) and annealed V_2O_5 films (see red graph) during the discharge process are shown in Fig. 8(c). The cycling data shows that as-sprayed and annealed V_2O_5 films show the highly reversible nature of Li insertion and extraction during the cycling. The capacity retention during discharge seems to be far better for the as-sprayed films during the cycling process. The V_2O_5 nanorods in the annealed films show higher capacity to begin with, however, the capacity fades faster relative to the as-sprayed films. For the annealed V_2O_5 films, the lower mass density following the anneal process may cause the faster decrease in capacity. During the anneal treatment,

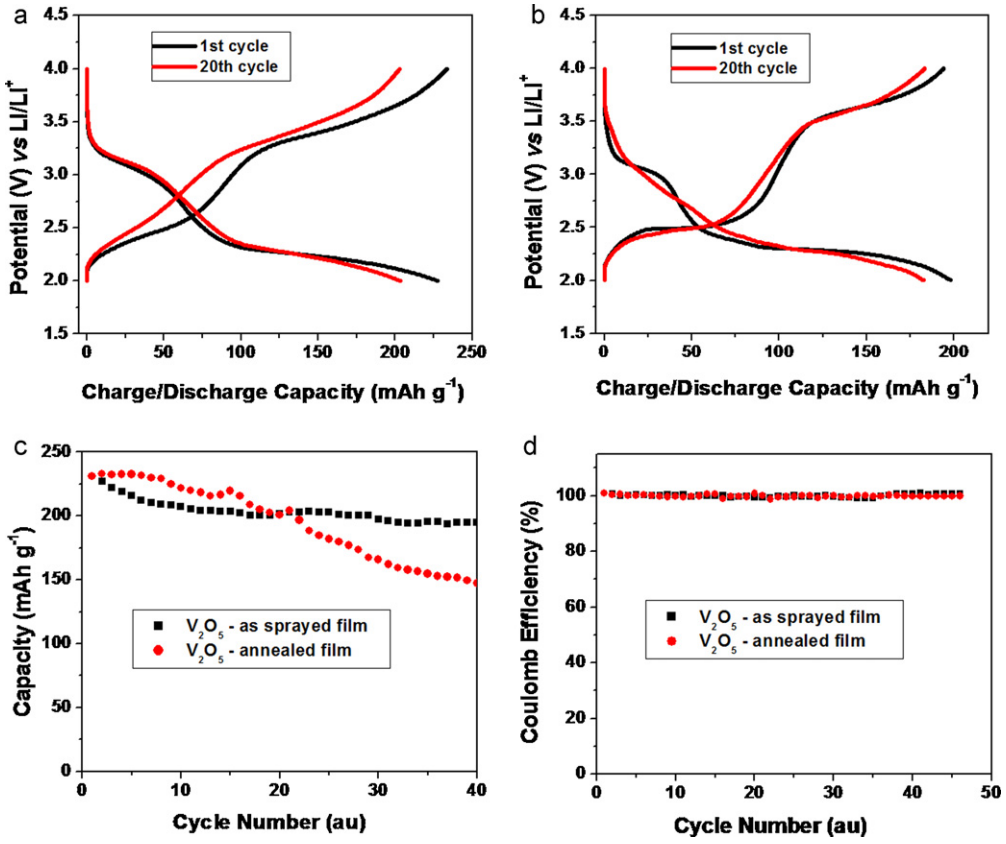

Fig. 8. Charge–discharge characteristics of electrodes from (a) as-sprayed V_2O_5 film and (b) V_2O_5 film annealed at 600 °C for 1 h in air, obtained at current density of ~0.025 mA cm^{-2}. (c) shows the cycling characteristics of electrodes from as-sprayed (black graph) and annealed (red graph) V_2O_5 films during the discharge process, and (d) shows Coulombic efficiency for electrodes from as-sprayed (black graph) and annealed (red graph) V_2O_5 films during the cycling process. (For interpretation of the references to color in this figure legend, the reader is referred to the web version of the article.)

as sprayed V_2O_5 films showed a weight loss (10–20%). Also, the transformation of V_2O_5 nanoparticles into nanorods leads to loss of particle–particle contacts inside the films and this in turn may lead to faster loss of capacity during cycling. The Coulombic efficiency (ratio of the discharge capacity to the charging capacity) for as-sprayed (black graph) and annealed (red graph) V_2O_5 films is shown in Fig. 8(d). The data shows high Coulombic efficiency (96–99%) for the cycling process during the lithium insertion–extraction cycles. A high Coulombic efficiency combined with good cycling behavior of V_2O_5 cathode films [27] is highly desired for practical commercial applications. Unlike the conventional electrodes, the ready to use film based electrodes reduce the cost factor involved in the electrode manufacturing process. The novel approach of plasma spray deposition presented in this report is a promising method in terms of reducing the process steps which constitute the electrode manufacturing. The solution plasma spray method affords direct deposition of V_2O_5 films ready for testing with minimal processing or treatment. In our approach we add binder/carbon to the films before testing, which constitutes as a necessary step. This may seem like a limitation of present approach, however, there are advantages. The solution plasma spray method provides direct deposition of V_2O_5 films eliminating several processing steps involved in cathode preparation such as slurry process and coating on the current collector. Furthermore, plasma spray deposition can also include *in situ* addition of carbon to the active electrode [28] and binder. The method also facilitates high throughput deposition and electrodes with large area could be realized for energy storage applications.

The observed capacity for the V_2O_5 films in our studies is lower relative to theoretical capacity. Earlier literature reports of V_2O_5 nanoparticles and nanorods show high capacity in the range 280–340 mAh g^{-1} [11,20,29]. This behavior could be explained by the fact that conventional electrodes invariably consist of carbon black, which acts as a conductive diluent. The observed capacity for our V_2O_5 films even at a lower rate was much lower than theoretical capacity of V_2O_5; this could be primarily due to low intrinsic electronic as well as ionic conductivity of V_2O_5 grains. These capacity values are however, significant, given the fact that V_2O_5 films were only soaked with a solution containing binder and carbon, and not physically homogenized using mechanical procedures such as slurry mixing or milling. One can attain faster ionic diffusion inside the V_2O_5 grains by controlling the particle size as well as the morphology so that majority of the particles are grown in a crystallographic direction, that offers least resistance for the Li-ion transport [11]. In order to address electronic conductivity limitations, Seng et al. investigated V_2O_5 electrodes with 5–30% multi-walled carbon nanotubes (MWNTs) and observed drastic improvement in capacity retention [30]. For better electronic conduction the carbon distribution should be uniform around the active material. We suppose *in situ* carbon incorporation during the plasma spray deposition of V_2O_5 films could help to improve the discharge capacity. Such an *in situ* plasma deposition approach has been developed for the synthesis of composite electrodes containing $LiFePO_4$ and carbon [28]. Using a similar approach, we are working on having carbon incorporated *in situ* during the plasma deposition process. This could be done by using carbonizing precursors such as acetylene during the spray deposition of V_2O_5 films. Having carbon incorporated *in situ* is expected to improve the conductivity of the films and that in turn will help improve the capacity and also cycleability.

4. Conclusions

In summary, we have successfully deposited the film based electrodes of V_2O_5 on substrates through plasma spray deposition using the solution precursors. Our approach affords direct deposition of the V_2O_5 films on large area substrates. Using an external injection approach the solution precursor is sprayed directly onto the Al or stainless steel current collectors. The XRD studies of the films showed the desired orthorhombic phase for V_2O_5. The microstructure of the as-sprayed films is made up of nanoparticles which are essentially in 20–50 nm range. Following the anneal treatment the as-sprayed films show the abundance of nanorods, which are well suited for electrode applications in Li batteries. The cyclic voltammetry studies on the as-sprayed and annealed V_2O_5 film based electrodes show that the kinetics of Li insertion and extraction is quite reversible. Both the V_2O_5 nanoparticles and the nanorods show the redox features characteristic of nanostructured V_2O_5 based film electrodes. The V_2O_5 film based electrodes show reversible discharge capacity in the range ~200–240 mAh g^{-1}. We have been working on further optimizations of our unique plasma approach to improve the discharge capacity. *In situ* impregnation of carbon into the V_2O_5 films during plasma deposition could help us achieve higher capacity and also improve cycling characteristics.

Acknowledgements

The authors acknowledge the free samples of separators from Celgard Inc and the test samples of carbon black from Timcal USA. One of the authors (JN) acknowledges the funding support from the Office of the Assistant Secretary for Energy Efficiency and Renewable Energy, Office of Vehicle Technologies of the U.S. Department of Energy.

Appendix A. Supplementary data

Supplementary data associated with this article can be found, in the online version, at doi:10.1016/j.jpowsour.2011.09.016.

References

[1] G.A. Nazri, G. Pistoia, Lithium Batteries: Science and Technology, Springer, 2009.
[2] J. Cho, C.S. Kim, S.I. Yoo, Electrochem. Solid State Lett. 3 (2000) 362–365.
[3] A.K. Padhi, K.S. Nanjundaswamy, J.B. Goodenough, J. Electrochem. Soc. 144 (1997) 1188–1193.
[4] J.M. Tarascon, M. Armand, Nature 414 (2001) 359–367.
[5] S.Y. Chung, J.S. Bloking, J.S. Chiang, Nat. Mater. 1 (2002) 123–128.
[6] Y. Wang, K. Takahashi, K. Lee, G.Z. Cao, Adv. Funct. Mater. 16 (2006) 1133–1144.
[7] E.A. Ponzio, T.M. Benedetti, R.M. Torresi, Electrochim. Acta 52 (2007) 4419–4427.
[8] H. Liu, Y. Wang, W. Yang, H. Zhou, Electrochim. Acta 56 (2011) 1392–1398.
[9] J. Muster, G.T. Kim, V. Krstic, J.G. Park, Y.W. Park, S. Roth, M. Burghard, Adv. Mater. 12 (2000) 420–424.
[10] T. Watanabe, Y. Ikeda, T. Ono, M. Hibino, M. Hosoda, K. Sakai, T. Kudo, Solid State Ionics 151 (2002) 313–320.
[11] N.A. Chernova, M. Roppolo, A.C. Dillonb, M.S. Whittingham, J. Mater. Chem. 10 (2009) 2526–2552.
[12] C. Delmas, S. Brethes, M. Menetrier, J. Power Sources 34 (1991) 113–118.
[13] C. Delmas, H. Cognac-Auradou, J.M. Cocciantelli, M. Menetrier, J.P. Doumerc, Solid State Ionics 69 (1994) 257–264.
[14] A. Vorobev, O. Zikanov, P. Mohanty, J. Phys. D: Appl. Phys. 41 (2008) 085302.
[15] P. Mohanty, A. George, L. Pollard, D. Snyder, J. Therm. Spray Technol. 19 (2010) 448–458.
[16] P. Mohanty, A.D. Roche, R.K. Guduru, V. Varadaraajan, J. Therm. Spray Technol. 19 (2010) 484–494.
[17] N.A. Moroz, H. Umapathy, P. Mohanty, J. Therm. Spray Technol. 19 (2010) 294–302.
[18] R.J. Cava, A. Santoro, D.W. Murphy, S.M. Zahurak, R.M. Fleming, P. Marsh, R.S. Roth, J. Solid State Chem. 65 (1986) 63–71.
[19] S.H. Ng, T.J. Patey, R. Buechel, F. Krumeich, J.Z. Wang, H.K. Liu, S.E. Pratsinis, P. Novak, Phys. Chem. Chem. Phys. 11 (2009) 3748–3755.
[20] A. Pan, J. Zhang, Z. Nie, G. Cao, B.W. Arey, G. Li, S. Liang, J. Liu, J. Mater. Chem. 20 (2010) 9193–9199.
[21] J. Patrissi, C.R. Martin, J. Electrochem. Soc. 146 (1999) 3176–3180.
[22] S.K. Martha, B. Markovsky, J. Grinblat, Y. Gofer, O. Haik, E. Zinigrad, D. Aurbach, T. Drezen, D. Wang., D. Deghenghi, I. Exnar, J. Electrochem. Soc. 156 (2009) A541–A552.
[23] A. Singhal, G. Skandan, G. Amatucci, F. Badway, N. Ye, A. Manthiram, H. Ye, J.J. Xu, J. Power Sources 129 (2004) 38–44.
[24] H.K. Song, K.T. Lee, M.G. Kim, L.F. Nazar, Adv. Funct. Mater. 20 (2010) 3818–3834.

[25] C.K. Chan, H. Peng, R.D. Twesten, K. Jarausch, X.F. Zhang, Y. Cui, Nano Lett. 7 (2007) 490–495.
[26] T. Gallasch, T. Stockhoff, D. Baither, G. Schmitz, J. Power Sources 196 (2011) 428–435.
[27] Y.Y. Liu, M. Clark, Q.F. Zhang, D.M. Yu, D.W. Liu, J. Liu, G.Z. Cao, Adv. Energy Mater. 1 (2011) 194–202.
[28] N.A. Moroz, B.C. Satishkumar, H. Umapathy, P. Mohanty, Adv. Funct. Mater., submitted for publication.
[29] C. Ban, N.A. Chernova, M.S. Whittingham, Electrochem. Commun. 11 (2009) 522–525.
[30] K.H. Seng, J.z. Liu, P. Guo, Z.X. Chen, D. Jia, H.K. Liu, Electrochem. Commun. 13 (2011) 383–386.